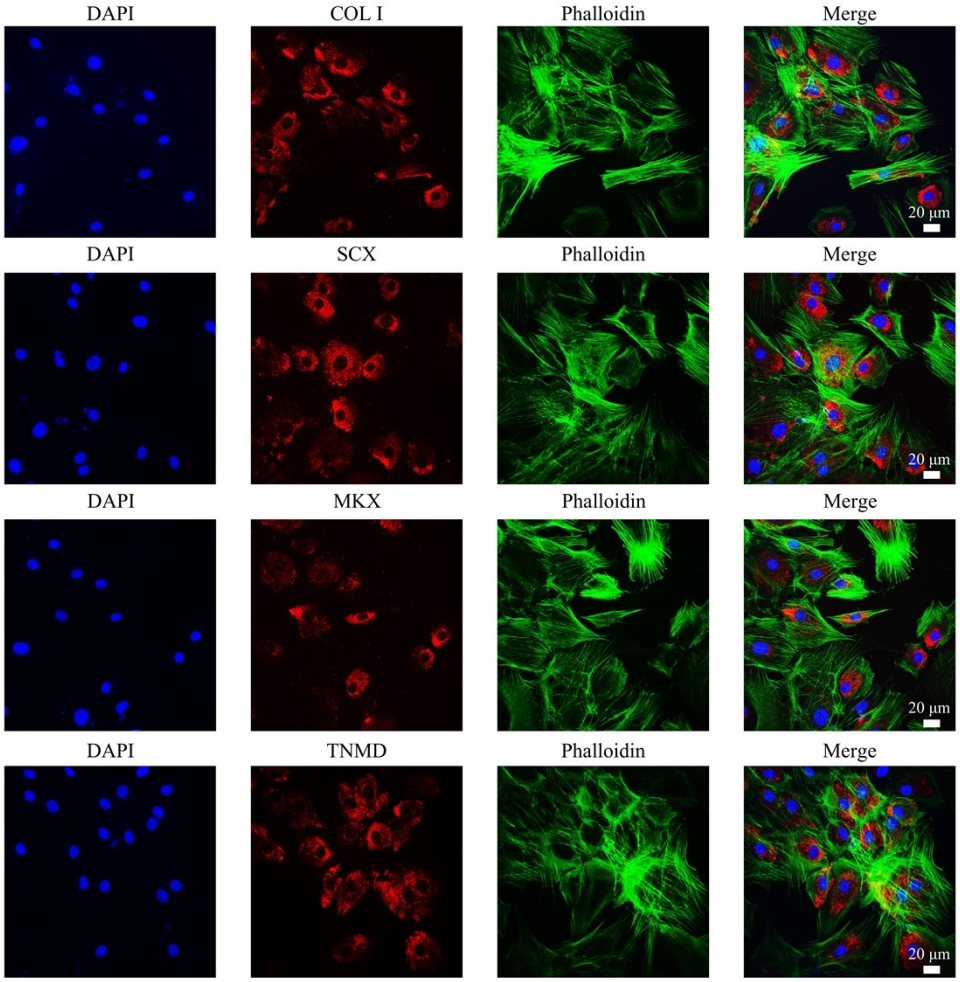


Figure S1 Immunofluorescence for different markers was used to identify the target cells as tendon stem cells.

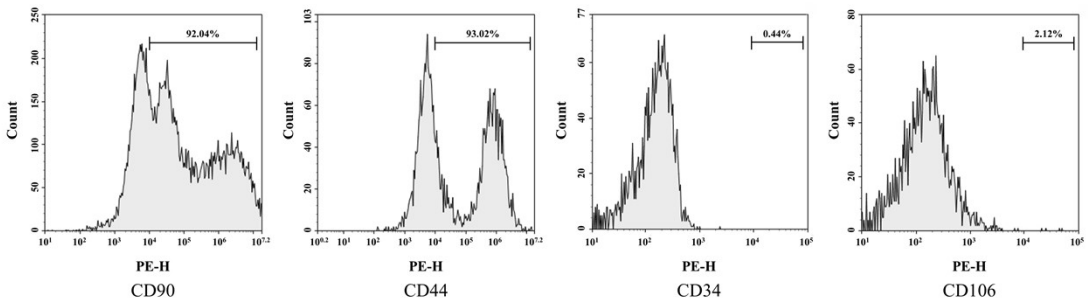


Figure S2 Characterization of acquired cells for tendon-derived stem cells using surface marker-based flow cytometry techniques.

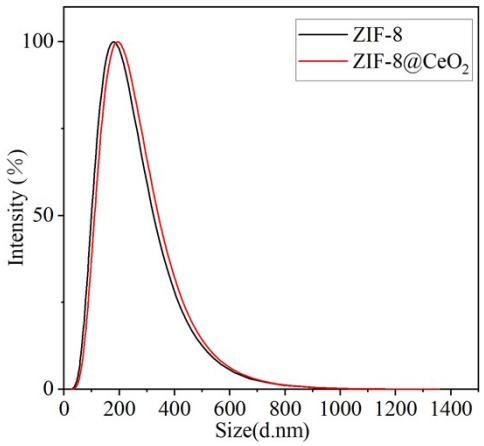


Figure S3 Probing the changes that occur in the particle size of ZIF-8 before and after it binds to $CeO_2$.

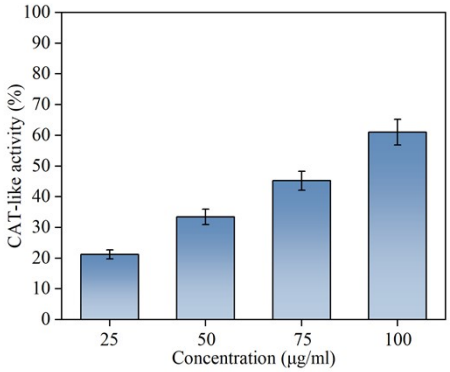


Figure S4 CAT activity under different concentrations of ZIF-8@$CeO_2$.

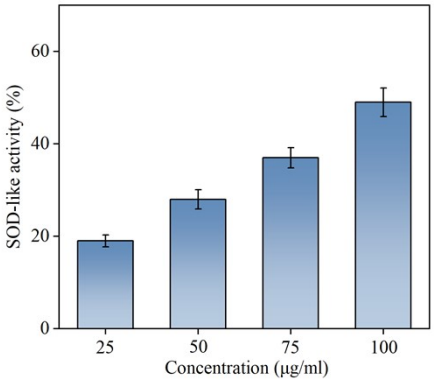

Figure S5 SOD activity under different concentrations of ZIF-8@$CeO_2$.

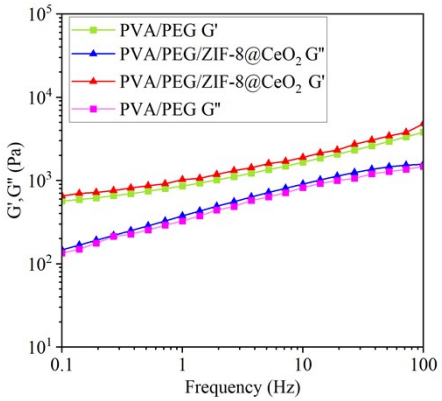


Figure S6 Frequency sweep dynamic rheological data for different samples.

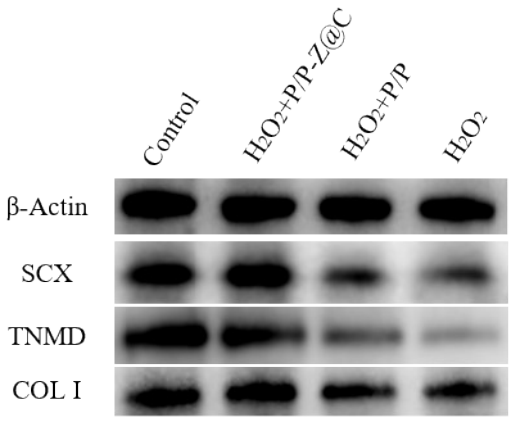


Figure S7 Protein expression of TNMD, SCX, and COL I in TDSCs of each group.

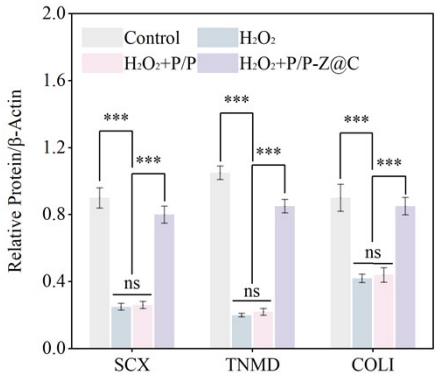


Figure S8 Protein quantification analysis of TNMD, SCX, and COL I in each group of

TDSCs.

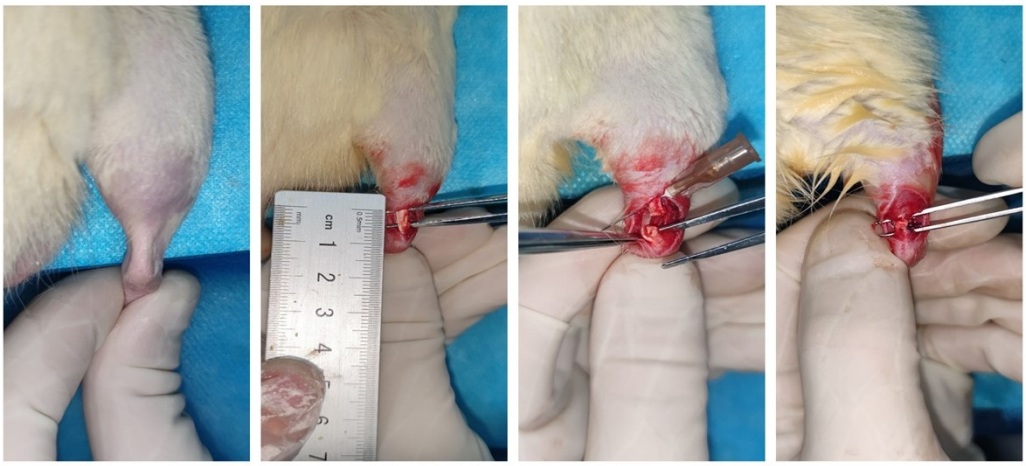

Figure S9 Construction and intervention in an animal model of Achilles tendon rupture.

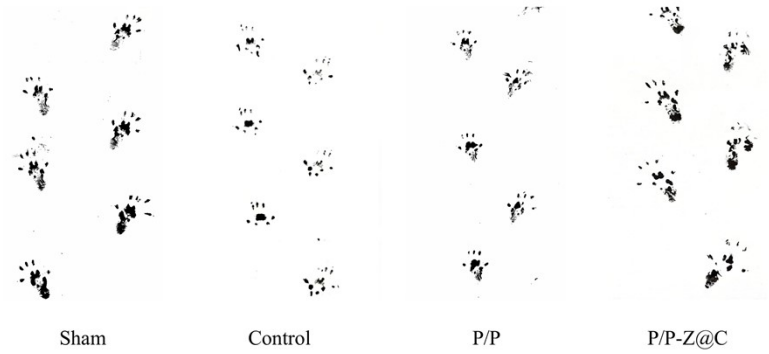


Figure S10 Gait analysis of rats in each group at 4 weeks postoperatively.

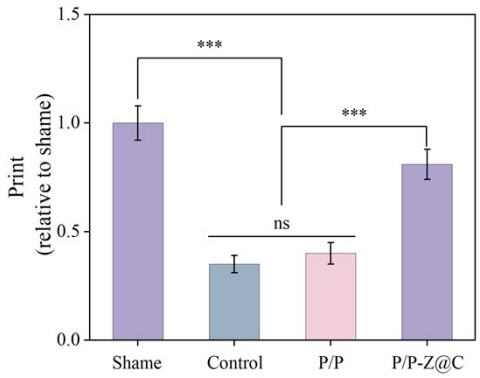


Figure S11 Quantification of paw print area in rats from each group 4 weeks

postoperatively.

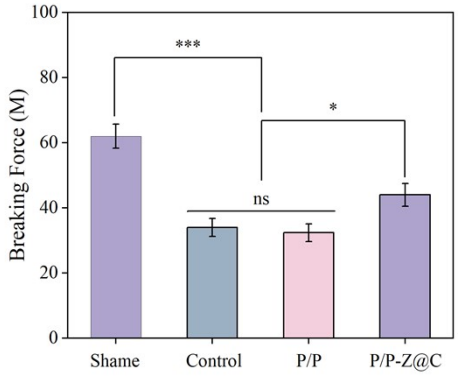


Figure S12 Maximum load on each group of tendons at 4 weeks postoperatively.

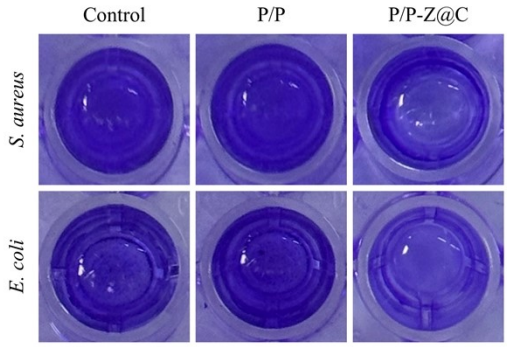


Figure S13 Crystal violet staining of bacterial biofilms after different hydrogel interventions.

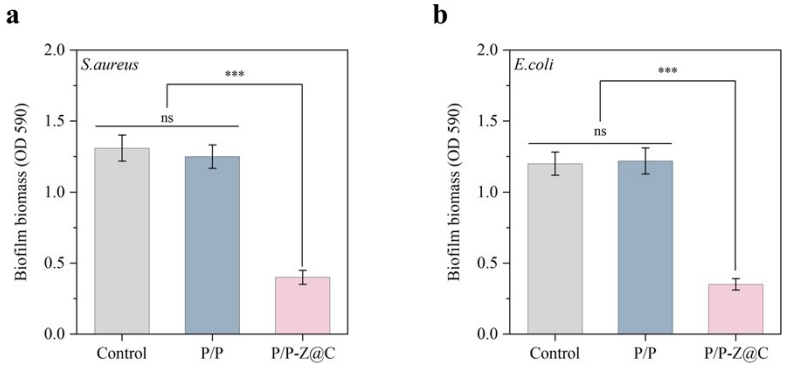


Figure S14 Quantitative analysis of crystal violet staining of bacterial biofilms.

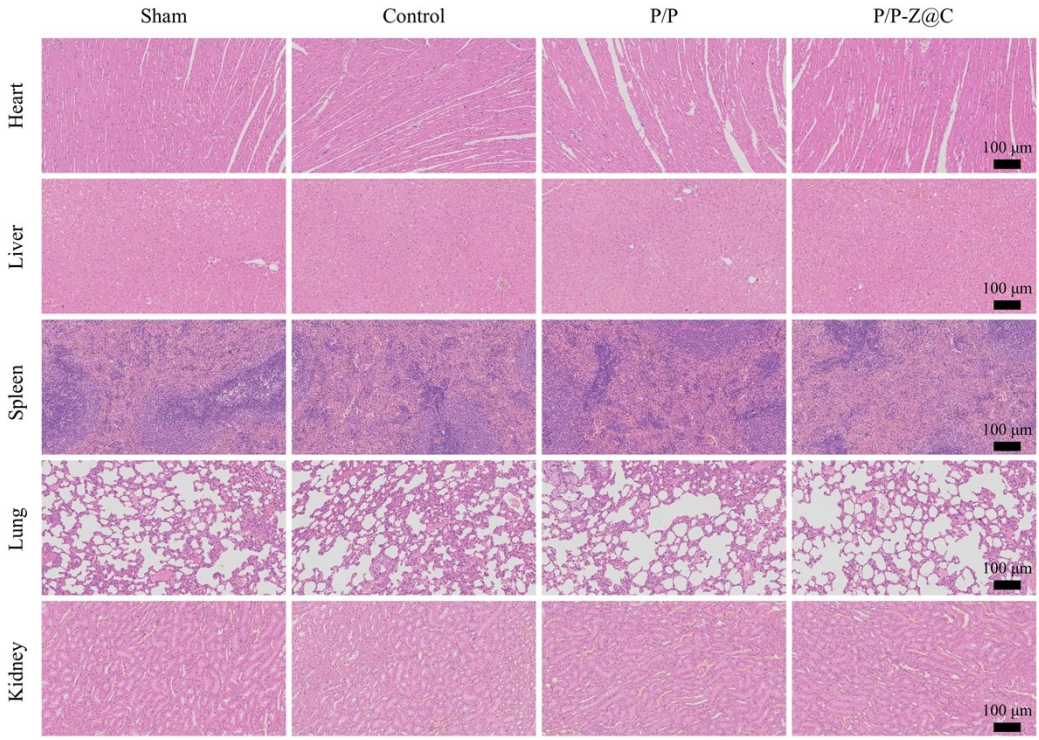


Figure S15 H&E staining of heart, liver, spleen, lung, and kidney tissues in vivo.